

**UNIVERSITY GRANTS COMMISSION  
BAHADUR SHAH ZAFAR MARG  
NEW DELHI – 110 002**

**PROFORMA FOR SUBMISSION OF INFORMATION AT THE TIME OF SENDING THE  
FINAL REPORT OF THE WORK DONE ON THE PROJECT**

1. Title of the Project **Studies on dye sensitized solar cells based on nanostructured titanium oxide**
2. NAME AND ADDRESS OF THE PRINCIPAL INVESTIGATOR **Dr. M. M. Karanjkar**
3. NAME AND ADDRESS OF THE INSTITUTION **Vivkeanand College, Tarabai Park, Kolhapur**
4. UGC APPROVAL LETTER NO. AND DATE: **47-423/12(WRO) dt 16<sup>th</sup> March 2013**
5. DATE OF IMPLEMENTATION **1<sup>st</sup> April 2013**
6. TENURE OF THE PROJECT **2 years**
7. TOTAL GRANT ALLOCATED Rs. **1,70,000/-**
8. TOTAL GRANT RECEIVED Rs. **1,40,000/-**
9. FINAL EXPENDITURE Rs. **1,69,797/-**
10. TITLE OF THE PROJECT **Studies on dye sensitized solar cells based on nanostructured titanium oxide**
11. OBJECTIVES OF THE PROJECT
  - Optimization of preparative parameters to synthesize aligned TiO<sub>2</sub> 1-D nanofibers
  - Study of structural, morphological and optical properties 1D-TiO<sub>2</sub> nanofibers
  - Fine tune of synthesis parameters of CdS shell and 1D-TiO<sub>2</sub> nanofibers
  - Characterization of core-shell structure to study their morphological, structural and optical properties
  - Sensitization of 1D-TiO<sub>2</sub>-CdS core-shell structure with semiconductor QDs like CdSe. PbS etc. in order to enhance the optical absorption and efficiency
  - To study solar cell performance of synthesized QDSSC

12. WHETHER OBJECTIVES WERE ACHIEVED **Yes**
13. ACHIEVEMENTS FROM THE PROJECT **1 paper published**
14. SUMMARY OF THE FINDINGS

Rutile titanium dioxide nanorods have been synthesized by a simple and cost-effective hydrothermal deposition method onto the conducting glass substrates. In order to study the effect of surfactants on the growth of TiO<sub>2</sub>, different surfactants like ethylenediaminetetraacetic acid, polyvinylpyrrolidone, cetyltrimethylammonium bromide and sodium dodecyl sulphate (SDS) are used. These films are characterized for their morphological, structural, compositional, optical and electrochemical properties using field emission scanning electron microscopy, X-ray diffraction, X-ray photoelectron spectroscopy, photoluminescence and electrochemical impedance spectroscopy techniques. FE-SEM images showed the formation of densely packed nanorods for SDS mediated TiO<sub>2</sub>. XRD patterns show the formation of polycrystalline TiO<sub>2</sub> with the tetragonal crystal structure possessing rutile phase. The chemical composition and valence states of the constituent elements were analysed by XPS. The films were photoelectrochemically active with the maximum current density of 378  $\mu\text{A}/\text{cm}^2$  with enhanced photovoltage of 615 mV for the sample prepared with SDS surfactant. Fig. 1 shows summary of results of TiO<sub>2</sub> samples.

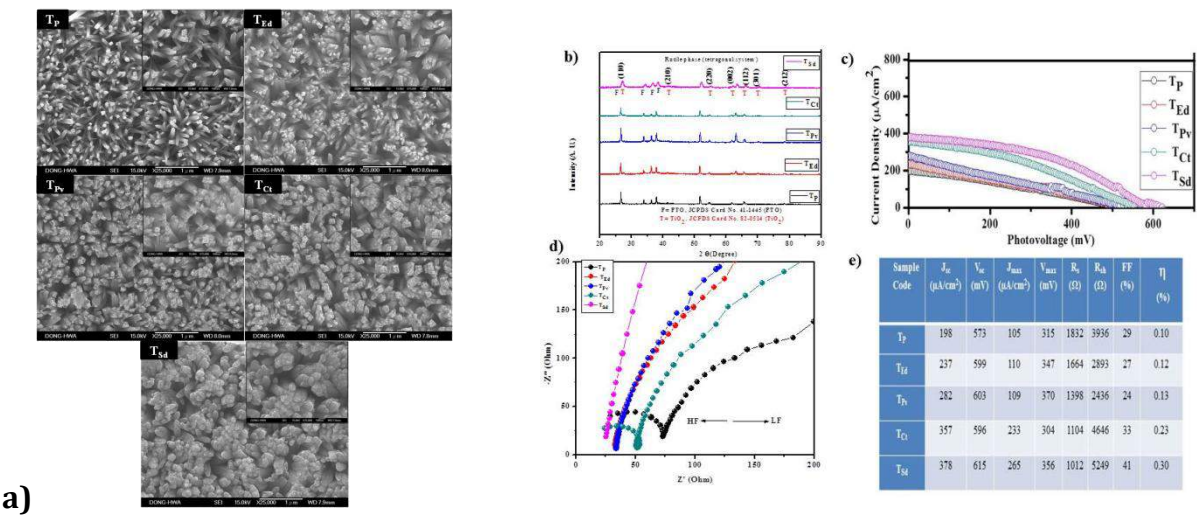


**Fig. 1** Summary of results of TiO<sub>2</sub> nanostructures a) FE-SEM images b) X-ray diffraction c) J-V measurements d) Impedance analysis and e) Table showing J-V parameters of different TiO<sub>2</sub> samples.

In summary, a facile hydrothermal method was developed to grow oriented single-crystalline rutile TiO<sub>2</sub> nanorod films on transparent conductive substrates. The growth parameters including the growth time, the growth temperature, the initial reactant concentration and types of additives could be selectively chosen to prepare TiO<sub>2</sub> nanorod

film with desired lengths and densities. The small lattice mismatch between the FTO substrate and rutile  $\text{TiO}_2$  plays a key role in driving the nucleation and growth of the rutile  $\text{TiO}_2$  nanorods on FTO. Due to  $\text{TiCl}_4$ -treatment, a light to electricity conversion efficiency of 0.30 % could be reached by employing SDS mediated rutile  $\text{TiO}_2$  nanorod film as the photoanode. PEC study of pristine and surfactant mediated  $\text{TiO}_2$  samples yielded a promising increase in the power conversion efficiency for sample TSd with highest current density  $378 \mu\text{A}/\text{cm}^2$  and the power conversion efficiency 0.30 % under  $100 \text{ mW}/\text{cm}^2$  illuminations.

A heterostructure of  $\text{TiO}_2/\text{CdS}$  is fabricated using hydrothermally grown  $\text{TiO}_2$  nanorods and successive ionic layer adsorption and reaction (SILAR) deposited CdS. Field Emission Scanning Electron Microscopy of  $\text{TiO}_2$ -CdS thin films show aggregated CdS QDs coverage onto the  $\text{TiO}_2$  nanorods. Under AM 1.5G illumination, we found the  $\text{TiO}_2$ -photoelectrode shows a power conversion efficiency of 1.75%, in an aqueous polysulfide electrolyte with short-circuit photocurrent density of  $4.04 \text{ mA}/\text{cm}^2$  which is higher than that of a bare  $\text{TiO}_2$  nanorods array. Fig. 2 shows the summary of results obtained for  $\text{TiO}_2/\text{CdS}$  heterostructure.

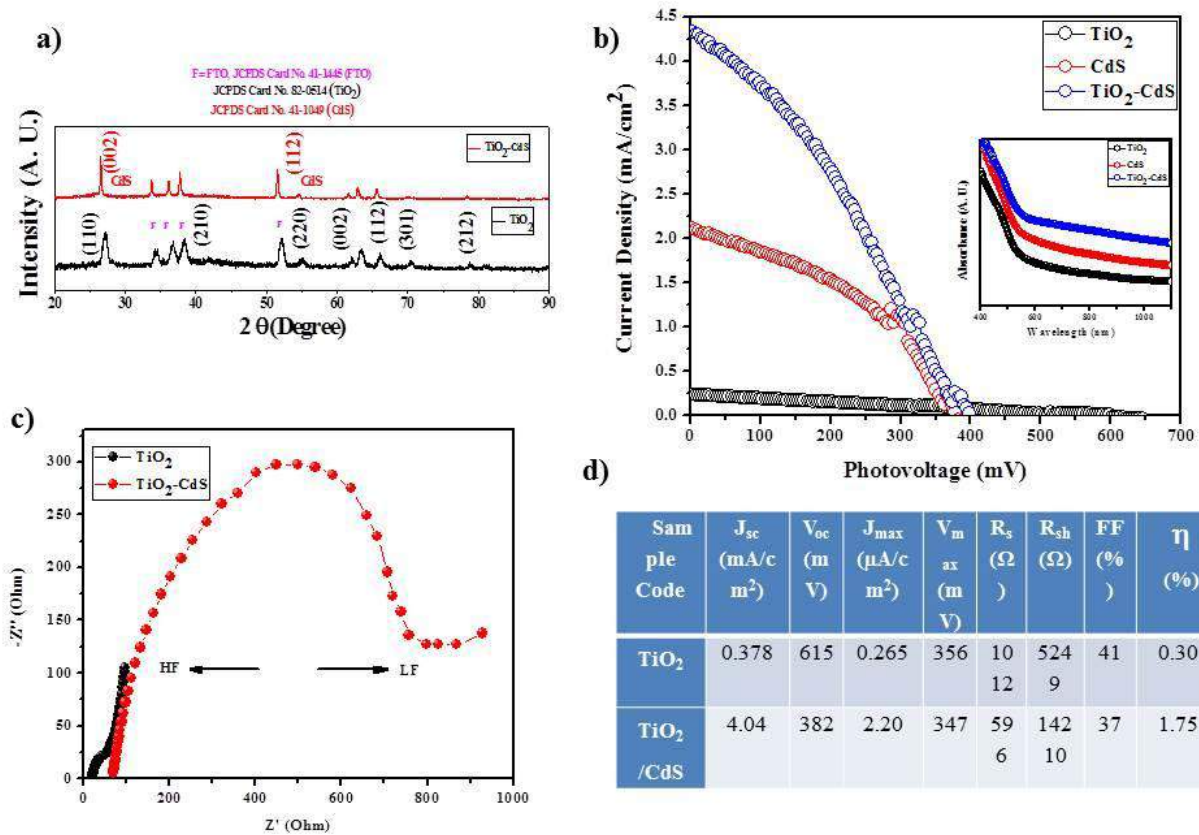


**Fig. 1** Summary of results of TiO<sub>2</sub>/CdS nanostructures a) X-ray diffraction b) J-V measurements c) Impedance analysis and d) Table showing J-V parameters.

TiO<sub>2</sub>-CdS is successfully fabricated through cost effective chemical routes such as hydrothermal, and SILAR. The stepwise band-edge structure in the TiO<sub>2</sub>-CdS heterojunction electrode creates an efficient charge transfer channel and triggers a high resistance to transport excited electrons back to the electrolyte, hence the photocurrents are improved.

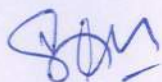
15. CONTRIBUTION TO THE SOCIETY

Today, about four fifth of India's need for electricity re met by fossile fuels which may best supply our needs of electricity for another 100-150 years. In India, the solar energy potential alone is many thousand times more than the total energy needs of the country. With over 300 sunny days in a year, India's geo-position allows her to receive over 5000 trillion kWh of pure solar energy every year, with the potential to generate huge quantity of electricity through a high energy security and zero-carbon process. Solar cell is a promising technology for addressing energy needs of India.

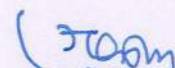
Solar cell is a key topic of energy technology research. Solar cells or photovoltaics directly converts sunlight into direct current (DC) electricity without going through any intermediate state. They are normally rugged, simple in design and need little maintenance. This technology can be used to electrify our villages. It can complement and supplement various energy needs in urban areas as well.

16. WHETHER ANY PH.D. ENROLLED/PRODUCED OUT OF THE PROJECT: No

17. NO. OF PUBLICATIONS OUT OF THE PROJECT: One



(PRINCIPAL INVESTIGATOR)



(PRINCIPAL)

**PRINCIPAL**

Vivekanand College,  
Kolhapur.

(Seal)



CO-INVESTIGATOR

**Professor,**  
**Department of Physics,**  
**Shivaji University,**  
**Kolhapur.**



# Photoelectrochemical solar cell based on surfactant mediated rutile TiO<sub>2</sub> nanorods

Sachin A. Pawar · D. S. Patil · U. T. Pawar ·  
R. S. Devan · M. M. Karanjkar · Y. R. Ma ·  
S. W. Shin · J. H. Kim · P. S. Patil

Received: 3 November 2014 / Accepted: 19 January 2015  
© Springer Science+Business Media New York 2015

**Abstract** Rutile titanium dioxide nanorods have been synthesized by a simple and cost-effective hydrothermal deposition method onto the conducting glass substrates. In order to study the effect of surfactants on the growth of TiO<sub>2</sub>, different surfactants like ethylenediaminetetraacetic acid, polyvinylpyrrolidone, cetyltrimethylammonium bromide and sodium dodecyl sulphate (SDS) are used. These films are characterized for their morphological, structural, compositional, optical and electrochemical properties using field emission scanning electron microscopy, X-ray diffraction, X-ray photoelectron spectroscopy, photoluminescence and electrochemical impedance spectroscopy techniques. FE-SEM images showed the formation of densely packed nanorods for SDS mediated TiO<sub>2</sub>. XRD patterns show the formation of polycrystalline TiO<sub>2</sub> with the tetragonal crystal structure possessing rutile phase. The chemical composition and valence states of the constituent

elements were analysed by XPS. The films were photoelectrochemically active with the maximum current density of 378  $\mu\text{A}/\text{cm}^2$  with enhanced photovoltage of 615 mV for the sample prepared with SDS surfactant.

## 1 Introduction

The addition of organic surfactants in the precursor solution is extremely important due to their influence on morphological and structural properties of material. Organic surfactants are commonly used in ZnO, TiO<sub>2</sub> to control the crystal shape and size, in order to produce high quality structure [1–3]. The role of the organic surfactants is to change the morphology of the deposit owing to their concentration-dependent specific activity during the growth of material. They are known to possess the unique ability to self-assemble into aggregates, such as micelles, which serve as templates during the deposition process [4, 5]. When the concentration approaches the critical micelle concentration (CMC) the bilayers or multilayers at the electrode interface are formed [6]. In aqueous medium micelles can form due to electrostatic force at the electrode surface even if the surfactant concentration is lower [7, 8]. Kamiko et al. [9] reported the surfactant effect of Ag on the thin film structure of TiO<sub>2</sub> by radio frequency magnetron sputtering. Uniform, debris-free, fewer-crack, and highly ordered TiO<sub>2</sub> nanotube arrays are prepared by Yang et al. [10] using surfactant-assisted vacuum impregnation approach. The influence of sodium dodecyl sulfate (SDS) as anionic surfactant and cetyltrimethylammonium bromide (CTAB) as cationic surfactant on the morphology, composition, and texture and corrosion behavior of electrodeposited Co-TiO<sub>2</sub> coatings was investigated by Shirani et al. [11].

S. A. Pawar · D. S. Patil · U. T. Pawar · P. S. Patil (✉)  
Thin Film Materials Laboratory, Department of Physics, Shivaji  
University, Kolhapur 416 004, M. S., India  
e-mail: patilps\_2000@yahoo.com

S. A. Pawar  
e-mail: sachinpawar69@gmail.com

R. S. Devan · Y. R. Ma  
Department of Physics, National Dong Hwa University,  
Hualien 97401, Taiwan

M. M. Karanjkar  
Department of Physics, Vivekanand College, Kolhapur, M. S.,  
India

S. W. Shin · J. H. Kim (✉)  
Department of Materials Science and Engineering, Chonnam  
National University, Gwangju 500 757, South Korea  
e-mail: jinhyeok@chonnam.ac.kr

Aligned single-crystalline and polycrystalline nanorod or nanowire films of wide band-gap semiconductor synthesis has attracted much attention because of their potential applications in novel photovoltaic devices including ordered hybrid bulk heterojunction as well as DSSCs and QDSSCs. Oriented nanorods or nanowires offer direct electrical pathways for photogenerated electrons and could increase the electron transport rate, which in turn may improve the light to power conversion efficiency of photovoltaic devices such as DSSCs or QDSSCs [12–18]. Polycrystalline transparent  $\text{TiO}_2$  nanotube array films demonstrate lower recombination. Uni-dimensional polycrystalline  $\text{TiO}_2$  nanostructures still show only slightly improved electron transport rate in DSSCs [19].

$\text{TiO}_2$  semiconductor is extensively studied due to wide band gap, environmental friendliness, low cost, its wide range of applications, such as DSSCs, QDSSCs, photocatalytic degradation of organic pollutants, hydrogen generation by water splitting, superhydrophobic and superhydrophilic materials [20–25]. Crystal structure, morphology and exposed facets play vital role in the performances of  $\text{TiO}_2$  in these applications. Hence, efforts have been devoted to tailor the crystal structure, morphology, and facets of  $\text{TiO}_2$  [26]. Quantum confinement effect governs the movement of electrons and holes in semiconductor nanomaterials, and the size and geometry of the materials has much importance for the transport properties related to phonons and photons.

In the present work, surfactant mediated growth of rutile  $\text{TiO}_2$  thin films using a facile and low cost hydrothermal method with nanorods formation is carried out. Transition of nanorods to bunch of nanorods takes place upon use of different surfactants; where bunch of nanorods formation is observed for  $\text{TiO}_2$  using SDS surfactant. The  $\text{TiO}_2$  films exhibit nanorods formation with compact structure over the entire substrate. Further, the effect of SDS surfactant leads to change in the morphological features. Effect of surfactants on the optical, structural, compositional and morphological characteristics of  $\text{TiO}_2$  is studied in detail. Photoelectrochemical study of  $\text{TiO}_2$  samples resulted into increase in the power conversion efficiency producing the maximum solar cell parameters for sample of SDS surfactant.

## 2 Experimental details

### 2.1 Thin film deposition

$\text{TiO}_2$  thin films are deposited on F:  $\text{SnO}_2$  (FTO) substrates by hydrothermal technique using titanium butoxide (TBT) precursor. All chemicals used were of analytical grade and used without further purification, double distilled water

served as a solvent for the whole chemical synthesis. In order to study effect of surfactants, ethylenediaminetetraacetic acid (EDTA), polyvinylpyrrolidone (PVP), CTAB and sodium dodecyl sulphate (SDS) surfactants from *s d fine chemicals* were used.

Initially the FTO substrate was subjected to  $\text{TiCl}_4$  seed layer formation in which the substrate was kept in a beaker of 0.1 M aqueous  $\text{TiCl}_4$  solution prepared using ice bath for 1 h at 60 °C.  $\text{TiCl}_4$  seeded FTO was rinsed with absolute ethanol and air annealed at 450 °C for 30 min. This  $\text{TiCl}_4$  seeded FTO is used further to carry out the  $\text{TiO}_2$  depositions. For the deposition of pristine  $\text{TiO}_2$  the typical recipe is: TBT (0.4 mL) was added to an equal volume of distilled water and concentrated hydrochloric acid (HCl). The resulting mixture was stirred for 30 min. The clear transparent solution was obtained which is then transferred to a Teflon-lined stainless steel autoclave of 30 mL volume, and a FTO was immersed in the solution inclined to the wall with the conducting surface facing downwards. The autoclave was sealed and placed in an oven at 180 °C for 3 h. The substrate (FTO) was removed from autoclave after cooling to room temperature and rinsed thoroughly using double distilled water and kept at room temperature for air drying. This thin film is finally air annealed at 450 °C for 30 min. Thus obtained  $\text{TiO}_2$  thin film is marked as  $T_p$ . In order to study the effect of surfactant on morphological evolution of  $\text{TiO}_2$  different surfactants were added in the  $\text{TiO}_2$  sol which is prepared using above recipe. Firstly, 0.1 M EDTA in 10 ml was dissolved in distilled water and subsequently added to the  $\text{TiO}_2$  sol. The resulting mixture was stirred for 30 min. The clear transparent solution was obtained. Thus obtained solution was used for autoclaving and preparing  $\text{TiO}_2$  thin films following the procedure as mentioned for pristine  $\text{TiO}_2$ . The obtained  $\text{TiO}_2$  thin film is marked as  $T_{Ed}$ . Likewise 0.1 M PVP, CTAB and SDS were added to pristine  $\text{TiO}_2$  sol respectively and the reactions were carried out as mentioned for  $T_p$  sample. These thin films were marked as  $T_{Pv}$ ,  $T_{Ct}$  and  $T_{Sd}$  respectively. Every time the temperature of the autoclave was kept constant at 180 °C and a deposition is carried out for 3 h and the thin films were air annealed after deposition at 450 °C for 30 min.

### 2.2 Characterization of $\text{TiO}_2$ thin films

Surface morphology was examined using FESEM (JEOL JSM-6500F). The elemental information of the films was analyzed using an XPS Thermo K-Alpha with multi-channel detector, which has high photonic energies from 0.1 to 3 keV. The XRD spectra of the films were recorded using X-ray powder diffractometer (Bruker AXS Analytical Instruments Pvt. Ltd., Germany, Model: D2 phaser). The room temperature optical absorption measurements

were performed in the wavelength range over 200–1,100 nm by using a UV–Vis spectrophotometer (UV1800, Shimadzu, Japan). The photoluminescence study was carried using Spectrofluorometer JASCO Model FP-750, Japan. The J–V curves were recorded on the Solar Simulator (model CT-150 AAA, Photoemission Tech, USA) under Air Mass 1.5G solar irradiations. For photoelectrochemical study the TiO<sub>2</sub> thin films (average area 0.30 cm<sup>2</sup>) and platinized FTO were employed as the working and counter electrodes, respectively. The distance between the photoelectrode and counter electrode was kept constant at 1 mm. An aqueous 0.1 M NaOH solution was used as the redox electrolyte. Measurements for the power output characteristics and J–V plots were made at fixed intervals after waiting a sufficient amount of time for the system to reach equilibrium (both in the dark and under illumination). Electrochemical impedance study was performed using the electrochemical workstation (ZIVE SP5) in the frequency range of 1,000–0.1 Hz with AC amplitude of 100 mV. An electrochemical cell was constituted using three electrode system, deposited film as a working electrode, platinum as a counter electrode and saturated calomel electrode (SCE) as a reference electrode.

### 3 Results and discussion

#### 3.1 Field emission scanning electron microscopy (FE-SEM)

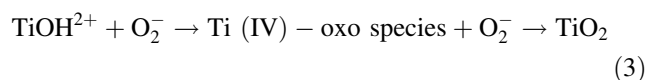
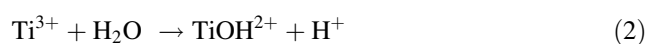
FESEM images in Fig. 1a shows the top view of the samples T<sub>P</sub>, T<sub>Ed</sub>, T<sub>Pv</sub>, T<sub>Ct</sub> and T<sub>Sd</sub> and inset shows high magnification FESEM images, respectively. Formation of nanorods with clearly visible textural boundaries for all the samples can be confirmed from the FESEM images. Initially for pristine TiO<sub>2</sub> sample (T<sub>P</sub>), nanorods formation took place with average diameter of 80–90 nm (Fig. 1a). These are separated nanorods and individual nanorod can be clearly distinguished. The addition of common surfactants including EDTA, PVP, CTAB and SDS had shown change in the surface morphology of TiO<sub>2</sub> nanorods [27]. However in the present case the density of nanorods found to increase from T<sub>P</sub>, to T<sub>Sd</sub>. For sample T<sub>Ed</sub>, 4–6 nanorods of average diameter 50–60 nm each are bound together. In case of samples T<sub>Pv</sub> and T<sub>Ct</sub> few nanorods are bound together to form bunch of nanorods similar to that of sample T<sub>Ed</sub> instead here the individual nanorod cannot be distinguished from each other. The average diameter of bunch of nanorods for samples T<sub>Pv</sub> and T<sub>Ct</sub> is 100–110 and 130–140 nm respectively. The density of nanorods in sample T<sub>Sd</sub> is much higher as compared to other three surfactants where number of nanorods (~4–6) have come

together forming a bunch of nanorods (with diameter ~600 nm) leading to the formation of TiO<sub>2</sub> nanoflowers. Figure 1 revealed that each bunch of nanorods in T<sub>Sd</sub> is assembled by 4–6 nanorods, which are larger than the nanorods of T<sub>P</sub>.

The nanorods provide high surface-to-volume ratio over the nanoparticles leading to enhanced photoelectrochemical properties.

##### 3.1.1 Growth mechanism

It is well known that the nanorods are tetragonal in shape with square top facets, the expected growth habit for the tetragonal crystal structure [28].



Initially Ti species from TBT precursor start to react with H<sup>+</sup> ions from concentrated solution. It is well known that Ti<sup>3+</sup> species are not stable in an aqueous solution, therefore TiOH<sup>2+</sup> species are formed by hydrolysis of Ti<sup>3+</sup>.

Species (Fig. 1b). According to the “dissolve and grow method” TiOH<sup>2+</sup> is oxidized to Ti(IV) by reaction with dissolved oxygen. The Ti(IV) complex ions are thus used as the growth units. The formation mechanism of the rutile TiO<sub>2</sub> NRs may be described as follows: For rutile TiO<sub>2</sub>, a TiO<sub>6</sub> octahedron forms first by bonding of a Ti atom and six oxygen atoms. The TiO<sub>6</sub> octahedron then shares a pair of opposite edges with the next octahedron, forming a chain-like structure. Because the growth rate of the different crystal faces depends on the numbers of corners and edges of the coordination polyhedra available, the growth of rutile nanorods follows the sequence (110) < (100) < (101) < (001).

In this case, rutile TiO<sub>2</sub> nanorods along [110] direction are formed. The nanorods are single crystalline.

Addition of SDS surfactant in the TiO<sub>2</sub> sol containing TBT leads to increased density of nanorods which give rise to bunch of nanorods. The faceted aligned nanorods have been observed for the films synthesized with the SDS, because SDS hinders the lateral growth and maintains high density of nanorods. It is suggested that, SDS promotes the ionic strength by dissolving in solution and consequently enhancing the solubility of the Ti species. After the formation of complex with Ti species, growth units of titania nanocrystals grow at step edges proceeded by the addition of Ti species. After dissolving in solution to it forms steady solutions, and then cap on the nanocrystal facets to enhance the orientation of particles after rutile particles were formed.



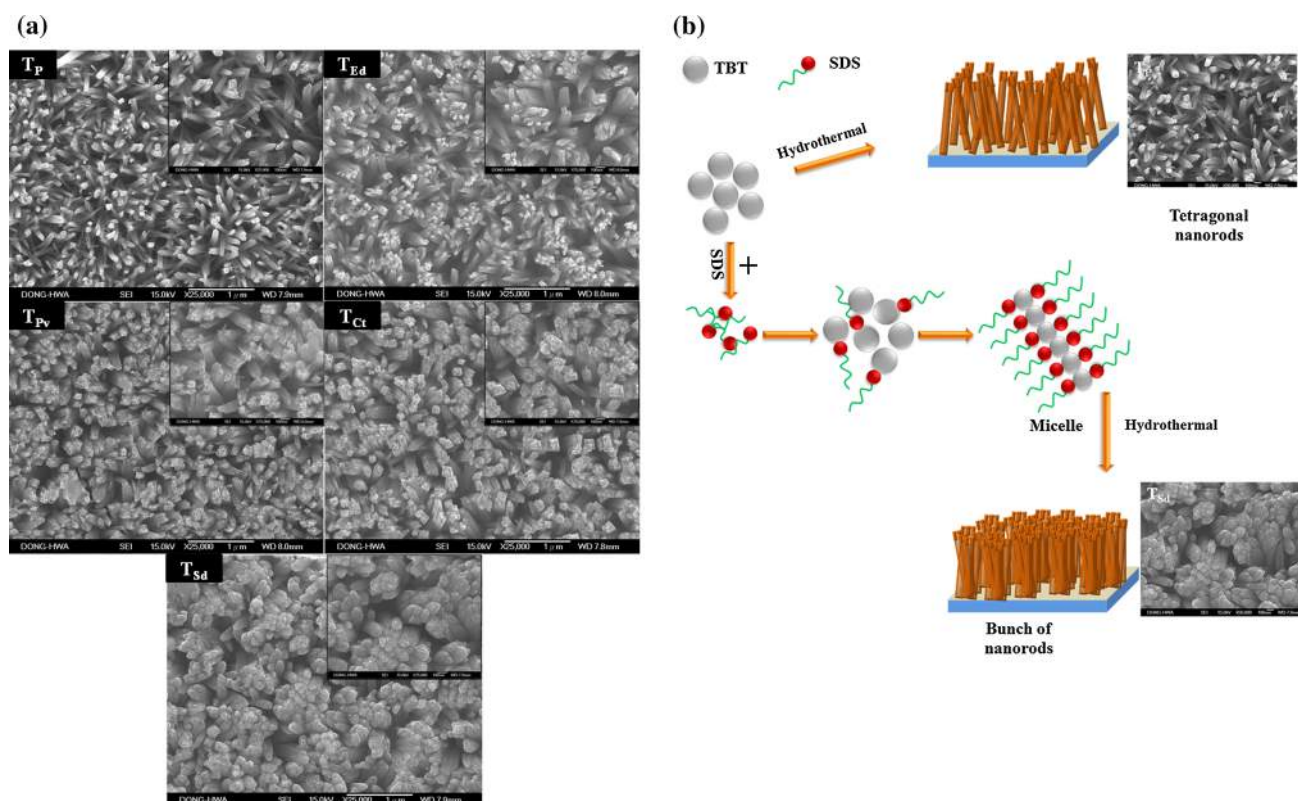


**Fig. 1** **a** FE-SEM images of rutile  $\text{TiO}_2$  nanorods synthesized using different surfactants at magnifications  $\times 25,000$  respectively. *Inset* shows FE-SEM at magnifications  $\times 75,000$ , **b** schematic illustration for the growth process of the  $\text{TiO}_2$  nanorods and bunch of  $\text{TiO}_2$  nanorods

### 3.2 X-ray photoelectron spectroscopy (XPS)

Quantitative analysis of the electronic structures and chemical properties of rutile  $\text{TiO}_2$  nanorods were performed by XPS. Figure 2 illustrates the  $\text{Ti}(2p)$  (in left panel) and  $\text{O}(1s)$  (in right panel) high resolution XPS spectra obtained for pristine  $\text{TiO}_2$  ( $T_P$ ) and SDS mediated  $\text{TiO}_2$  ( $T_{Sd}$ ) samples, respectively. Left panel of Fig. 2 shows the double peak feature in the  $\text{Ti}(2p)$  spectra for  $T_P$  and  $T_{Sd}$  samples, suggesting the presence of element ‘Ti’ in  $\text{TiO}_2$  nanorod structures. However, to precisely determine the features of the double peaks of  $\text{Ti}(2p_{3/2})$  and  $\text{Ti}(2p_{1/2})$ , the  $\text{Ti}(2p)$  XPS spectra for the samples  $T_P$  and  $T_{Sd}$  shown in left panel were decomposed via Voigt curve fitting function within the Shirley background. For all samples decomposition resulted into perfect fit for only two peaks. These two decomposed peaks of the samples  $T_P$  and  $T_{Sd}$  are located at the binding energy of 457.6 eV (peak a1), 458.56 eV (peak a2), and 463.30 eV (peak b1), 464.22 eV (peak b2) corresponding to the  $\text{Ti}(2p_{3/2})$  and  $\text{Ti}(2p_{1/2})$  core levels respectively, of  $\text{Ti}^{4+}$  cations of  $\text{TiO}_2$  crystal structure. No displacement has been observed in the peak position of the peak a1, a2 and b1, b2. These peak positions are akin to those reported by Pawar et al. [29] and Mali et al. [30] for  $\text{TiO}_2$  thin films. The energy separation between these two peaks for all studied samples is

$\sim 10$  eV, which is akin to that observed in  $\text{TiO}_2$  nanomaterials by Thind et al. [31].

Likewise right panel shows compound double peak feature in the  $\text{O}(1s)$  spectra for samples  $T_P$  and  $T_{Sd}$ , suggesting the presence of element ‘O’ in  $\text{TiO}_2$  rutile nanorods. A very strong O 1s peak coupled with a small shoulder was observed in all studied samples. The decomposition of these O (1s) spectra resulted into two peaks, an intense peak centered at 528.84 eV (peak c1), 529.78 eV (peak c2) and a small peak at 531.06 eV (peak d1), 531.57 eV (peak d2), respectively. No displacement has been observed in the peak position of the peak c1, c2. An intense peak observed in the spectra corresponds to  $\text{O}^{2-}$  anions and is characteristic of the Ti-oxide. The small peak observed at the vicinity of intense oxygen [O(1s)] peak indicates the surface contamination [32–34] or presence of O containing species, such as hydroxyl groups or water molecules that are adsorbed on the surface of the sample [35]. This clearly indicates that synthesized hierarchical structures consisted of only the elements Ti and O of pure  $\text{TiO}_2$ .

### 3.3 X-ray diffraction (XRD)

$\text{TiO}_2$  exhibits anatase, rutile or brookite phase with the tetragonal crystal structure. Figure 3 show the XRD

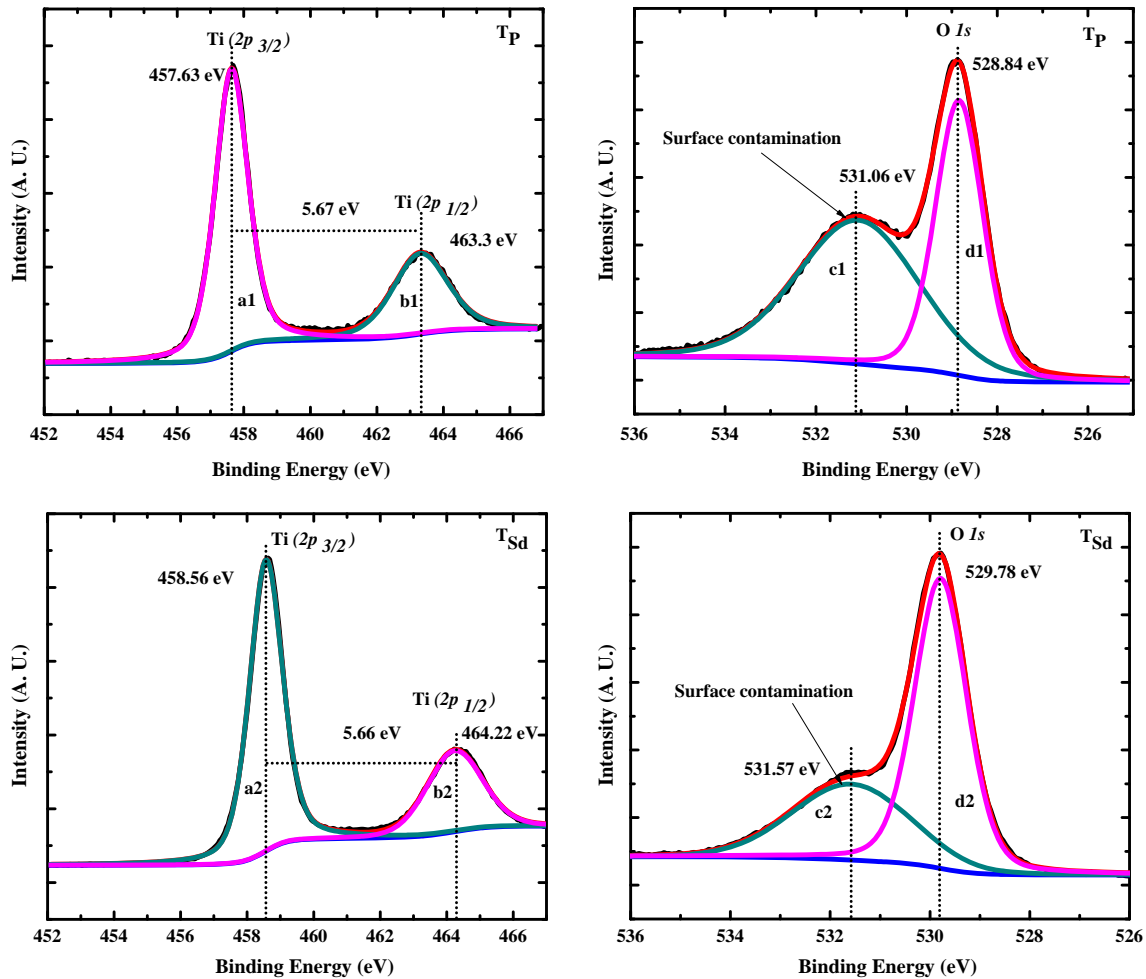


**Fig. 2** High-resolution XPS spectra of the Ti 2p (left panel) and O (1s) (right panel) core levels of the pristine TiO<sub>2</sub> (T<sub>P</sub>) and T<sub>Sd</sub> samples respectively. The XPS spectra are decomposed via Voigt curve fitting

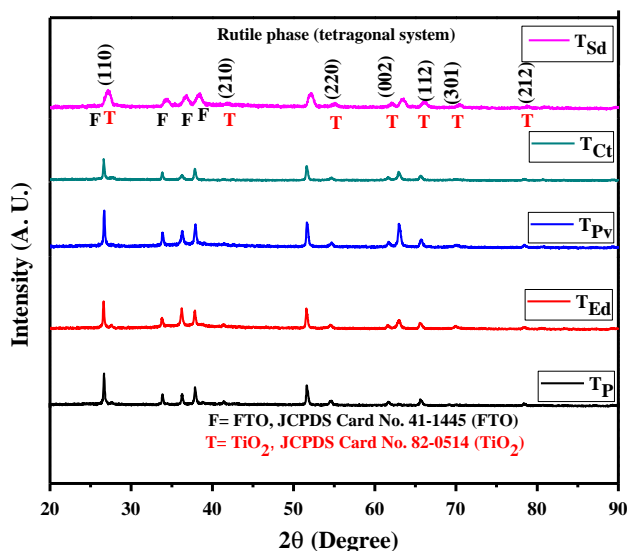


**Fig. 3** X-ray diffraction patterns of TiO<sub>2</sub> samples T<sub>P</sub>, T<sub>Ed</sub>, T<sub>Pv</sub>, T<sub>Ct</sub> and T<sub>Sd</sub>

patterns of hydrothermally grown pristine TiO<sub>2</sub> (T<sub>P</sub>) and surfactant mediated TiO<sub>2</sub> i.e., of samples T<sub>Ed</sub>, T<sub>Pv</sub>, T<sub>Ct</sub> and T<sub>Sd</sub> respectively.

The comparison of observed XRD patterns with the standard JCPDS data (82-0514) confirms the formation of a rutile TiO<sub>2</sub> phase with tetragonal crystal structure space group: P4<sub>2</sub>/mmn (136). No peaks of anatase or brookite phase are detected, indicating the high purity of the products. Many workers have reported that hydrothermally deposited TiO<sub>2</sub> thin films are either anatase [36] or rutile [37]. All the TiO<sub>2</sub> thin films exhibit the polycrystalline nature having major peak corresponding to (110) plane as highest intense peak. Besides these major peaks, six more peaks corresponding to (210), (220), (002), (112), (301) and (212) etc., planes are observed. The lattice parameters 'a' and 'c' for TiO<sub>2</sub> are determined for tetragonal structure by the following expression [38];

$$d_{hkl} = \frac{a}{\sqrt{h^2 + k^2 + l^2 \left(\frac{a^2}{c^2}\right)}} \quad (4)$$

The observed mean values of lattice parameters  $a = 4.5080 \text{ \AA}$  and  $c = 3.027 \text{ \AA}$  are in good agreement with the standard lattice parameters  $a = 4.5937 \text{ \AA}$  and  $c = 2.9587 \text{ \AA}$  respectively affirming the crystal system to be tetragonal.

By applying the Scherrer formula

$$D = \frac{0.9\lambda}{\beta \cos \theta} \quad (5)$$

on the rutile (110) diffraction peaks, the average crystallite sizes of the samples were found to be 26, 47, 62, 91 and 125 nm for the samples  $T_P$ ,  $T_{Ed}$ ,  $T_{Pv}$ ,  $T_{Ct}$  and  $T_{Sd}$  respectively. This result indicated that the crystal sizes of the resulting rutile nanorods increased with addition of different surfactants and is highest for SDS surfactant which is also supported by the FESEM images.

### 3.4 Photoluminescence (PL)

Figure 4 shows the PL spectra of  $\text{TiO}_2$  thin films of pristine  $\text{TiO}_2$  and of prepared by using different surfactants. We have carried out room temperature PL measurement of  $\text{TiO}_2$  thin films with an excitation wavelength of 325 nm.

All samples showed a broad PL band in 350–550 nm region, which could be assigned to the radiative recombination of self-trapped exciton [39, 40]. Three main emission peaks appear at 352, 411 and 450 nm which corresponds to 3.52, 3.01 and 2.75 eV respectively. Furthermore, shoulders 411 and 450 nm are also observed, although with very low intensity.

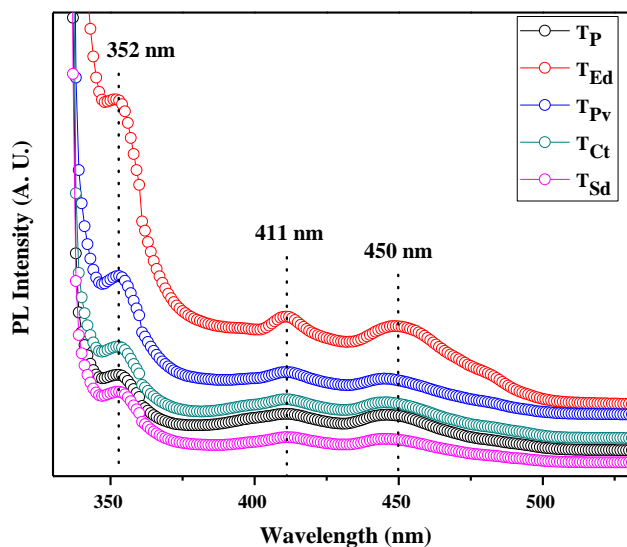


**Fig. 4** Room temperature photoluminescence spectra of  $\text{TiO}_2$  samples  $T_P$ ,  $T_{Ed}$ ,  $T_{Pv}$ ,  $T_{Ct}$  and  $T_{Sd}$  showing an undefined trend in intensity with respect to different surfactants. The dotted lines are drawn at the corresponding values of emission peaks

Pristine and surfactant mediated  $\text{TiO}_2$  samples show broad emission peaks centered around 430 nm originating from defect levels of these samples [41]. In our case this emission peak is observed around 450 nm. An increased emission in the spectra range of above 450 nm is usually attributed to PL from  $\text{TiO}_2$  surface states [42]. Some PL peaks in the region 411–459 nm can be attributed to recombination of photoinduced electrons and holes. The energy of sharp peak at 450 nm is very close to the trap energy levels located at 0.64 eV [43] below the conduction band, which was attributed to the oxygen vacancies with trapped electrons (F-center) [44]. The oxygen vacancies are a kind of intrinsic defects in  $\text{TiO}_2$  lattice forming intermediate energy levels within  $\text{TiO}_2$  band gap [45], which act as recombination centers for photoinduced electrons and holes. Therefore this emission can arise from the  $e^-h^+$  recombination via oxygen vacancies.

### 3.5 J–V measurement

The J–V characteristics of the films were recorded using a solar simulator of a class AAA (Photo emission Tech., USA, Model-CT 150) under AM 1.5 G solar irradiations with a two-electrode configuration using a xenon arc lamp ( $100 \text{ mW/cm}^2$ ). During I–V measurements the active area of the device was kept  $0.30 \text{ cm}^2$ ; therefore for calculation of power conversion efficiency the  $P_{in}$  was taken as  $100 \text{ mW/cm}^2 \times 0.30 \text{ cm}^2 = 30 \text{ mW}$ . The following cell configuration was used to record J–V plots: glass/FTO/ $\text{TiO}_2$ /NaOH/Pt-FTO/glass.

Figure 5 shows the J–V characteristics of samples  $T_P$ ,  $T_{Ed}$ ,  $T_{Pv}$ ,  $T_{Ct}$  and  $T_{Sd}$ . The magnitude of the  $J_{sc}$  was 198, 237, 282, 357 and  $378 \mu\text{A/cm}^2$  for the samples  $T_P$ ,  $T_{Ed}$ ,  $T_{Pv}$ ,  $T_{Ct}$  and  $T_{Sd}$ , respectively. The corresponding  $V_{oc}$  was found to be 573, 599, 603, 596 and 615 mV, respectively. This observation reveals that the  $J_{sc}$  gives different values for different surfactant but for SDS surfactant i.e., for

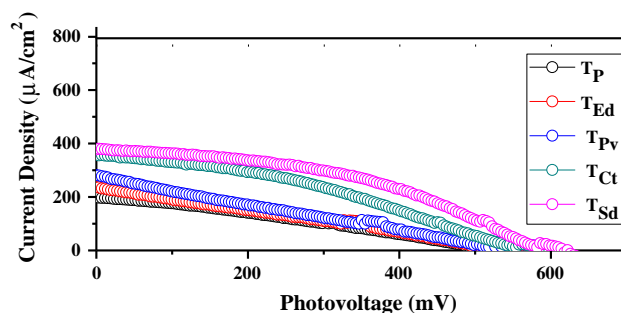


**Fig. 5** Increase in the current density for different surfactants is observed for photoelectrochemical performance of  $\text{TiO}_2$  samples  $T_P$ ,  $T_{Ed}$ ,  $T_{Pv}$ ,  $T_{Ct}$  and  $T_{Sd}$

sample T<sub>Sd</sub> it shows maximum photocurrent of 378  $\mu\text{A}/\text{cm}^2$ , with  $V_{\text{oc}}$  of 615 mV.

Various solar cell parameters that are obtained from the power output are listed in Table 1. The smaller value of  $R_{\text{sh}}$  in the case of all samples is responsible for the deviation from the ideal J–V characteristics and thereby low fill factor.

The values of  $R_{\text{s}}$  and  $R_{\text{sh}}$  are calculated from J–V curves and the variation in  $R_{\text{s}}$  and  $R_{\text{sh}}$  is summarized in Table 1.  $R_{\text{s}}$  varies from 903 to 1,198  $\Omega$ , while  $R_{\text{sh}}$  changes from 2,436 to 5,249  $\Omega$ . The T<sub>Sd</sub> sample deposited by hydrothermal method with the highest photoconversion efficiency 0.30 % is obtained. This value is higher than pure TiO<sub>2</sub> thin films reported by us in the past [29]. However, further improvements, are inevitable.

The enhancement in the photoelectrochemical parameters of sample T<sub>Sd</sub> is due to following reasons. Each grown TiO<sub>2</sub> aligned nanostructures can provide notably high surface area, which is essential to produce high photocurrent. Such substantial increment in current is due to high surface area offered by the bunch of nanorods architecture of rutile TiO<sub>2</sub>. The increase in  $J_{\text{sc}}$  can be attributed to better injection or charge collection efficiency of oriented rutile TiO<sub>2</sub> nanorods. Further, rutile TiO<sub>2</sub> has advantages of higher chemical stability and higher refractive index [46]. In general, oriented 1D-nanostructures, such as rutile TiO<sub>2</sub> nanorods, are believed to be able to enhance the performance of solar cells since they provide quick charge separation and continuous confined pathways for charge carriers transport towards electrodes with increased mobility [47]. These advantages, further complemented by the low cost template-free one pot facile hydrothermal synthesis, which make it very interesting to make use of these rutile TiO<sub>2</sub> nanorods arrays in solar cells.

The nanorod morphology of TiO<sub>2</sub> offers a large internal surface area with no concomitant decrease in geometric and structural order. The vertical orientation of the crystalline nanorod arrays makes them excellent electron percolation pathways for efficient, vectorial charge transport along the nanorod axis [48]. The ordered architectures help to reduce the electron recombination and function as the direct pathway for fast electron transport to the charge

collecting electrode. In addition, further improved PCE could be with the consideration of the following factors: (1) ideal TiO<sub>2</sub> nanorods grown perpendicular to the FTO substrates via manipulating the densities of TiO<sub>2</sub> nanorods, and (2) the single-crystalline structure of the nanorods allows a fast and efficient transfer of the photogenerated electrons to the collected FTO substrate, which can effectively suppress the recombination of electrons and holes.

### 3.6 Electrochemical impedance spectroscopy (EIS)

Electrochemical impedance spectroscopy (EIS) has been regarded as a powerful technique to characterize the carrier transport, electronic and ionic processes and recombination in photoelectrochemical solar cell. EIS was employed to study the photo-electrochemical kinetics of the surfactant mediated rutile TiO<sub>2</sub> thin films.

In order to study the effect of surfactant additives in TBT on the conversion efficiency of rutile TiO<sub>2</sub>, EIS measurement of all the TiO<sub>2</sub> samples were conducted in the dark using 0.1 M NaOH electrolyte with applied forward bias voltage  $-0.6$  V. The measuring AC frequency range was 1,000–0.1 Hz. Figure 6a shows the Nyquist plots of samples T<sub>P</sub>, T<sub>Ed</sub>, T<sub>Pv</sub>, T<sub>Ct</sub> and T<sub>Sd</sub> and an equivalent circuit as shown in inset of Fig. 6a is proposed to fit the spectra. These plots are well fitted into one semicircle using the Nova 9.1 software in terms of an appropriate equivalent circuit composed of constant phase elements (Q) and resistors (R) (Fig. 6b). The smaller semicircle at high frequency was attributed to electron transfer at the interface of electrolyte and Pt-FTO counter electrode while the straight line at lower frequency was associated with electron transport in the TiO<sub>2</sub> electrode and electron back reaction at the interface of the TiO<sub>2</sub> photoanode and the electrolyte [49–51]. The electrochemical parameters derived from the fitting are summarized in Table 2, this includes charge transfer resistances ( $R_{\text{pt}}$ ) at the Pt-FTO counter/electrolyte interface and charge transfer resistances ( $R_{\text{ct}}$ ) related to photoexcited electron hole recombination at the TiO<sub>2</sub>/electrolyte. The equivalent circuit elements have the following meaning:  $R_{\text{s}}$  is the series resistance, or a solution resistor. The sample T<sub>Sd</sub> has  $R_{\text{s}} = 985 \Omega/\text{cm}^2$  and

**Table 1** Various solar cell parameters obtained for the glass/FTO/TiO<sub>2</sub>/NaOH/Pt-FTO/glass system are summarized in the table

Sample	$J_{\text{sc}}$ ( $\mu\text{A}/\text{cm}^2$ )	$V_{\text{oc}}$ (mV)	$J_{\text{max}}$ ( $\mu\text{A}/\text{cm}^2$ )	$V_{\text{max}}$ (mV)	$R_{\text{s}}$ ( $\Omega$ )	$R_{\text{sh}}$ ( $\Omega$ )	FF (%)	Efficiency, $\eta$ (%)
T <sub>P</sub>	198	573	105	315	1,153	3,936	29	0.10
T <sub>Ed</sub>	237	599	110	347	1,164	2,893	27	0.12
T <sub>Pv</sub>	282	603	109	370	1,198	2,436	24	0.13
T <sub>Ct</sub>	357	596	233	304	1,004	4,646	33	0.23
T <sub>Sd</sub>	378	615	265	356	903	5,249	41	0.30

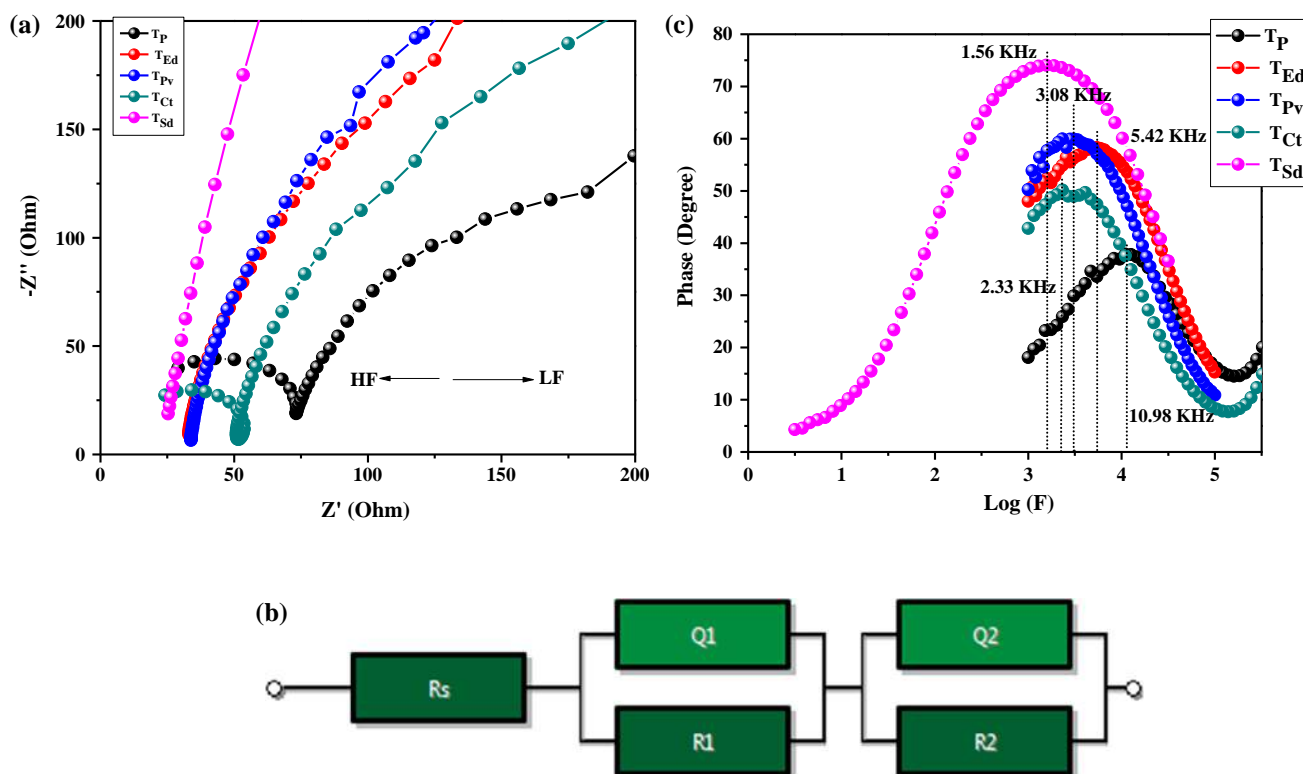


**Fig. 6** **a** Impedance spectra of samples  $T_P$ ,  $T_{Ed}$ ,  $T_{Pv}$ ,  $T_{Ct}$  and  $T_{Sd}$  and Pt/FTO-glass counter electrode, measured in the dark under  $-0.60$  V applied bias, **b** equivalent circuit used to analyze EIS data and **c** bode

plot of rutile  $TiO_2$  samples  $T_P$ ,  $T_{Ed}$ ,  $T_{Pv}$ ,  $T_{Ct}$  and  $T_{Sd}$  to determine electron lifetime in  $TiO_2$

**Table 2** Various EIS parameters obtained for the glass/FTO/ $TiO_2$ /NaOH/Pt-FTO/glass system are summarized in the table

Sample	$R_s$ ( $\Omega/cm^2$ )	$R_1$ ( $\Omega/cm^2$ )	$Q_1$ (mF)	$R_2$ ( $\Omega/cm^2$ )	$Q_2$ (mF)	$\tau_e$ ( $\mu s$ )
$T_P$	47.1	1,541	9.08	1,207	187	14
$T_{Ed}$	47.3	1,331	21.74	805	232	29
$T_{Pv}$	46.6	1,210	42.13	598	311.9	51
$T_{Ct}$	46.2	1,058	64.20	580	286.1	68
$T_{Sd}$	46.1	985	103.00	454	349.8	102

$R_2 = 454 \Omega/cm^2$  which is much lower than the rest of the  $TiO_2$  samples. A likely reason for this phenomenon is that more electrons were injected into the conduction band of  $TiO_2$  nanorods [52] which is in accordance with the increase in  $J_{sc}$  values. This leads to an increase in the recapture of electrons into the conduction band of titania nanorods by NaOH. This indicates that the sample  $T_{Sd}$  is more conducting than  $T_P$ ,  $T_{Ed}$ ,  $T_{Pv}$  and  $T_{Ct}$  samples which thereby produces the highest values of the photocurrent and photovoltage upon illumination amongst all the  $TiO_2$  samples studied in this report. Moreover  $TiO_2$ /electrolyte and Pt-FTO/electrolyte interface for  $T_{Sd}$  sample shows least electron diffusion resistance.

In order to calculate the electron lifetime Bode plot is used which is obtained from EIS data (Fig. 6c). The maximum frequencies ( $\omega_{max}$ ) from the Bode plots of the

$T_P$ ,  $T_{Ed}$ ,  $T_{Pv}$ ,  $T_{Ct}$  and  $T_{Sd}$  are 10.98, 5.42, 3.08, 2.33 and 1.56 kHz respectively. Since ( $\omega_{max}$ ) is inversely associated with the electron lifetime ( $\tau_e$ ):  $\tau_e = 1/(2\pi f)$  [53, 54] the decreased  $\omega_{max}$  indicates a reduced rate of the charge-recombination process of the  $TiO_2$  samples. The electron lifetime is found to increase from 14 to 102  $\mu s$  for samples  $T_P$  to  $T_{Sd}$ .

From the EIS results, it is clear that the charge recombination rate is the rate determining step of the  $TiO_2$  device performance, since decreased charge recombination rate from samples  $T_P$  to  $T_{Sd}$  resulted in an improvement of the device performance, in that order. From these results, we can conclude that charge recombination of  $T_{Sd}$  is slower than that of other  $TiO_2$  samples. Further, inhibition of back electron transfer from the  $TiO_2$  to electrolyte ions gives a higher  $V_{oc}$ .



## 4 Conclusions

In summary, a facile hydrothermal method was developed to grow oriented single-crystalline rutile TiO<sub>2</sub> nanorod films on transparent conductive substrates. The growth parameters including the growth time, the growth temperature, the initial reactant concentration and types of additives could be selectively chosen to prepare TiO<sub>2</sub> nanorod film with desired lengths and densities. The small lattice mismatch between the FTO substrate and rutile TiO<sub>2</sub> plays a key role in driving the nucleation and growth of the rutile TiO<sub>2</sub> nanorods on FTO. Due to TiCl<sub>4</sub>-treatment, a light to electricity conversion efficiency of 0.30 % could be reached by employing SDS mediated rutile TiO<sub>2</sub> nanorod film as the photoanode.

PEC study of pristine and surfactant mediated TiO<sub>2</sub> samples yielded a promising increase in the power conversion efficiency for sample T<sub>sd</sub> with highest current density 378  $\mu\text{A}/\text{cm}^2$  and the power conversion efficiency 0.30 % under 100 mW/cm<sup>2</sup> illuminations.

**Acknowledgments** One of the authors S.A.P. wishes to acknowledge the UGC-SAP-DSA-I, New Delhi and Department of Science and Technology (DST) INDIA for financial support through DST-PURSE scheme. This work is partially supported by the Human Resource Development of the Korea Institute of Energy technology Evaluation and Planning (KETEP) grant funded by the Korea Government Ministry of knowledge Economy (No. 20124010203180). D.S.P. wishes to acknowledge the DST, New Delhi, INDIA for financial support through Women Scientist Scheme-A (WOS-A) project.

## References

- R.C. Pawar, J.S. Shaikh, A.A. Babar, P.M. Dhere, P.S. Patil, *Sol. Energy* **85**, 1119 (2011)
- R.C. Pawar, J.S. Shaikh, N.L. Tarwal, M.M. Karanjkar, P.S. Patil, *J. Mater. Sci. Mater. Electron.* **23**, 349 (2012)
- J. Yang, L. Pan, G. Zhu, X. Liu, H. Sun, Z. Sun, *J. Electroanal. Chem.* **677–680**, 101 (2012)
- Y. Ying, C.P. Mehnert, M.S. Wong, *Angew. Chem.* **38**, 58 (1999)
- S. Manne, J.P. Cleveland, H.E. Gaub, G.D. Stucky, P.K. Hansma, *Langmuir* **10**, 4409 (1994)
- U. Retter, M. Tchachnikova, *J. Electroanal. Chem.* **550**, 201 (2003)
- K.M. Kadish, G.B. Maiya, C. Araullo, R. Guillard, *Inorg. Chem.* **28**, 2725 (1989)
- J.F. Liu, W.A. Ducker, *J. Phys. Chem. B* **103**, 8558 (1999)
- M. Kamiko, K. Aotani, R. Suenaga, J.W. Koo, J.G. Ha, *Vacuum* **86**, 438 (2011)
- Z. Yang, D. Pan, C. Xi, J. Li, J. Shi, F. Xu, Z. Ma, *J. Power Sources* **236**, 10 (2013)
- A. Shirani, M. Momenzadeh, S. Sanjabi, *Surf. Coat. Technol.* **206**, 2870 (2012)
- B.A. Gonfa, H. Zhao, J. Li, J. Qiu, M. Saidani, S. Zhang, R. Izquierdo, N. Wu, M.A.E. Khakani, D. Ma, *Sol. Energy Mater. Sol. Cells* **124**, 67 (2014)
- S.S. Mali, H. Kim, C.S. Shim, W.R. Bae, N.L. Tarwal, S.B. Sadale, P.S. Patil, J.H. Kim, C.K. Hong, *Cryst. Eng. Commun.* **15**, 5660 (2013)
- S.S. Mali, H. Kim, P.S. Patil, C.K. Hong, *Dalton Trans.* **42**, 16961 (2013)
- R.C. Pawar, J.S. Shaikh, P.S. Shinde, P.S. Patil, *Mater. Lett.* **65**, 2235 (2011)
- B.H. Lee, M.Y. Song, S.Y. Jang, S.M. Jo, S.Y. Kwak, D.Y. Kim, *J. Phys. Chem. C* **113**, 21453 (2009)
- X.Y. Yu, J.Y. Liao, K.Q. Qiu, D.B. Kuang, C.Y. Su, *ACS Nano* **5**, 9494 (2011)
- G. Zhu, L. Pan, T. Xu, Z. Sun, *J. Electroanal. Chem.* **659**, 205–208 (2011)
- K. Zhu, N.R. Neale, A. Miedaner, A.J. Frank, *Nano Lett.* **7**, 69 (2007)
- B. O'Regan, M. Graetzel, *Nature* **353**, 737 (1991)
- K. Murakoshi, G. Kano, Y. Wada, S. Yanagida, H. Miyazaki, M. Matsumoto, S. Murasawa, *J. Electroanal. Chem.* **396**, 27 (1995)
- S. Izadyar, S. Fatemi, *Ind. Eng. Chem. Res.* **52**, 10961 (2013)
- S.K. Choi, S. Kim, S.K. Lim, H. Park, *J. Phys. Chem. C* **114**, 16475 (2010)
- Y. Wang, B. Li, T. Liu, C. Xu, Z. Ge, *Colloids Surf. A* **441**, 298 (2014)
- L. Gong, L. Zhang, N. Wang, J. Li, S. Ji, H. Guo, G. Zhang, Z. Zhang, *Sep. Purif. Technol.* **122**, 32 (2014)
- R.S. Devan, R.A. Patil, J.H. Lin, Y.R. Ma, *Adv. Funct. Mater.* **22**, 3326 (2012)
- B. Liu, E.S. Aydil, *J. Am. Chem. Soc.* **131**, 3985 (2009)
- S.S. Mali, H. Kim, C.S. Shim, P.S. Patil, J.H. Kim, C.K. Hong, *Sci. Rep.* **3**, 3004 (2013)
- S.A. Pawar, R.S. Devan, D.S. Patil, V.V. Burungale, T.S. Bhat, S.S. Mali, S.W. Shin, J.E. Ae, C.K. Hong, Y.R. Ma, J.H. Kim, P.S. Patil, *Electrochim. Acta* **117**, 470 (2014)
- S.S. Mali, R.S. Devan, Y.R. Ma, C.A. Betty, P.N. Bhosale, R.P. Panmand, B.B. Kale, S.R. Jadhav, P.S. Patil, J.H. Kim, C.K. Hong, *Electrochim. Acta* **90**, 666 (2013)
- S.S. Thind, G. Wu, M. Tian, A. Chen, *Nanotechnology* **23**, 475706 (2012)
- J.A. Rengifo-Herrera, E. Mielczarski, N.C. Castillo, J. Kiwi, C. Pulgarin, *Appl. Catal. B* **84**, 448 (2008)
- R.S. Devan, W.D. Ho, C.H. Chen, H.W. Shiu, C.H. Ho, C.L. Cheng, S.Y. Wu, Y. Liou, Y.R. Ma, *Nanotechnology* **20**, 445708 (2009)
- R.S. Devan, W.D. Ho, S.Y. Wu, Y.R. Ma, *J. Appl. Crystallogr.* **43**, 498 (2010)
- R.S. Devan, C.L. Lin, S.Y. Gao, C.L. Cheng, Y. Liou, Y.R. Ma, *Phys. Chem. Chem. Phys.* **13**, 13441 (2011)
- X.H. Yang, Z. Li, C. Sun, H.G. Yang, C. Li, *Chem. Mater.* **23**, 3486 (2011)
- M. Ye, H.Y. Liu, C. Lin, Z. Lin, *Small* **9**, 312 (2013)
- B.D. Cullity, *Elements of X-ray Diffraction* (Addison Wesley, Reading, 1956)
- F.J. Knorr, C.C. Mercado, J.L. Mchale, *J. Phys. Chem. C* **112**, 12786 (2008)
- J. Ng, S. Xu, X. Zhang, H.Y. Yang, D.D. Sun, *Adv. Funct. Mater.* **20**, 4287 (2010)
- R. Sasikala, A.R. Shirole, S.R. Bharadwaj, *J. Colloid Interface Sci.* **409**, 135 (2013)
- N.M. Rahman, K.M. Krishna, T. Soga, T. Jimbo, M. Umeno, *J. Phys. Chem. Solids* **60**, 201 (1999)
- N. Serpone, D. Lawless, R. Khairutdinov, *J. Phys. Chem.* **99**, 16646 (1995)
- K.V. Baiju, A. Zachariah, S. Shukla, S. Biju, M.L.P. Reddy, K.G.K. Warriar, *Catal. Lett.* **130**, 130 (2009)
- A. Janotti, J.B. Varley, P. Rinke, N. Umezawa, G. Kresse, C.G. Van de Walle, *Phys. Rev. B* **81**, 085212 (2010)
- K.J. Kim, K.D. Benkstein, J. van de Lagemaat, A.J. Frank, *Chem. Mater.* **14**, 1042 (2002)

47. H. Liu, D. Ding, C. Ning, Z. Li, *Nanotechnology* **23**, 015502 (2012)
48. M. Law, L.E. Greene, J.C. Johnson, R. Saykally, P.D. Yang, *Nat. Mater.* **4**, 455 (2005)
49. J. Wang, Z. Lin, *Chem. Mater.* **22**, 579 (2010)
50. J.Y. Kim, K.J. Lee, S.H. Kang, J. Shin, Y.E. Sung, *J. Phys. Chem. C* **115**, 19979–19985 (2011)
51. K.H. Park, T.Y. Kim, J.H. Kim, H.J. Kim, C.K. Hong, J.W. Lee, *J. Electroanal. Chem.* **708**, 39 (2013)
52. G. Dai, L. Zhao, J. Li, L. Wan, F. Hu, Z. Xu, B. Dong, H. Lu, S. Wang, J. Yu, *J. Colloid Interface Sci.* **365**, 46 (2012)
53. S. Lee, I.S. Cho, J.H. Lee, D.H. Kim, D.W. Kim, J.Y. Kim, H. Shin, J.K. Lee, H.S. Jung, N.G. Park, K. Kim, M.J. Ko, K.S. Hong, *Chem. Mater.* **22**, 1958 (2010)
54. J. Bisquert, F. Fabregat-Santiago, I. Mora-Sero, G. Garcia-Belmonte, S. Gimenez, *J. Phys. Chem. C* **113**, 17278 (2009)